Available online at www.sciencedirect.com
ScienceDirect
C. R. Geoscience 338 (2006) 908–916
COMPTES RENDUS GEOSCIENCE
http://france.elsevier.com/direct/CRAS2A/

Geomaterials / Géomatériaux

Transport coefficients of saturated compact clays

Marcin Paszkuta, Maria Rosanne, Pierre M. Adler *

Sisyphe, 4, place Jussieu, 75252 Paris cedex 05, France

Received 20 May 2005; accepted after revision 23 June 2006

Available online 4 August 2006

Written on invitation of the Editorial Board

Abstract

The coefficients that characterize the simultaneous transports of mass, heat, solute and current through compact clays are experimentally and theoretically determined. The role of a characteristic length scale that can be derived from conductivity and permeability is illustrated for the electrokinetic coefficients. The macroscopic Soret coefficient in clays was found five times larger than in the free fluid, presumably because of extra couplings with electrical phenomena. ***To cite this article: M. Paszkuta et al., C. R. Geoscience 338 (2006).***

Résumé

Coefficients de transport pour des argiles compactes saturées. Les coefficients qui caractérisent le transport simultané de masse, de chaleur, de soluté et de courant au travers d'argiles compactes sont déterminés expérimentalement et théoriquement. Le rôle d'une longueur caractéristique qui peut être déduite de la conductivité et de la perméabilité est illustré pour ce qui concerne les coefficients électrocinétiques. Le coefficient de Soret macroscopique dans les argiles est cinq fois plus grand que dans le fluide libre, probablement à cause de couplages supplémentaires avec les phénomènes électriques. ***Pour citer cet article : M. Paszkuta et al., C. R. Geoscience 338 (2006).***

Keywords: Compact clays; Electro-osmotic coefficient; Soret coefficient

Mots-clés : Argiles compactes ; Coefficient électro-osmotique ; Coefficient de Soret

1. Introduction

The ability of clay soils to act as semipermeable membranes that inhibit the passage of electrolytes may be of great value. Clays exhibit membrane properties when charged ionic species are excluded from the pores, while uncharged species have a relatively free movement. Clays are therefore capable of inducing coupled transport such as osmosis, electro-osmosis, electrodialysis, and thermodiffusion.

The major purpose of this work was to experimentally determine the coefficients that characterize these couplings in compact clays. More precisely, let us consider a porous medium filled by an electrolyte solution with a concentration n (defined as the number of molecules per m^3). When a pressure gradient ∇P, an electric field $\mathbf{E}$, a concentration gradient ∇n, and a temperature

* Corresponding author.
E-mail address: padler@ccr.jussieu.fr (P.M. Adler).

1631-0713/$ – see front matter
doi:10.1016/j.crte.2006.06.008

gradient ∇T are simultaneously applied to the porous medium, four fluxes are generated, namely a flow characterized by the seepage velocity $\mathbf{U}$ ($\mathrm{m\,s^{-1}}$), a current density $\mathbf{I}$ ($\mathrm{A\,m^{-2}}$), a solute flux $\mathbf{J}_\mathrm{d}$ which is the number of particles per unit surface and per unit time ($\mathrm{m^{-2}\,s^{-1}}$), and an heat flux $\mathbf{J}_\mathrm{q}$ ($\mathrm{W\,m^{-2}}$). Close to equilibrium, when gradients are not too large, the problem is linear, and fluxes are proportional to these gradients (see [4]). Then, with respect to the solvent-fixed reference plane, one can write:

$$\mathbf{I} = \gamma_{11}\cdot\mathbf{E} + \gamma_{12}\cdot(-\nabla\mathbf{P}) + \gamma_{13}\cdot(-\nabla\mathbf{n}) + \gamma_{14}\cdot(-\nabla\mathbf{T}) \tag{1a}$$

$$\mathbf{U} = \gamma_{21}\cdot\mathbf{E} + \gamma_{22}\cdot(-\nabla\mathbf{P}) + \gamma_{23}\cdot(-\nabla\mathbf{n}) + \gamma_{24}\cdot(-\nabla\mathbf{T}) \tag{1b}$$

$$\mathbf{J}_\mathrm{d} = \gamma_{31}\cdot\mathbf{E} + \gamma_{32}\cdot(-\nabla\mathbf{P}) + \gamma_{33}\cdot(-\nabla\mathbf{n}) + \gamma_{34}\cdot(-\nabla\mathbf{T}) \tag{1c}$$

$$\mathbf{J}_\mathrm{q} = \gamma_{41}\cdot\mathbf{E} + \gamma_{42}\cdot(-\nabla\mathbf{P}) + \gamma_{43}\cdot(-\nabla\mathbf{n}) + \gamma_{44}\cdot(-\nabla\mathbf{T}) \tag{1d}$$

A distinction is generally made between the diagonal phenomenological coefficients γ_{ij} with $i = j$, and the non-diagonal ones with $i \neq j$. Because of the Onsager symmetry properties, the non-diagonal coefficients are not all independent.

A literature search shows that measurements of these coefficients for clays (and especially for compact clays) were not frequently performed. Interesting contributions concerning electrokinetic coefficients are from Elrick et al. [5], Gronevelt et al. [6] and Sherwood and Craster [19]. To the best of our knowledge, only Thornton and Seyfried [20], and Lerman [10] have contributed to thermodiffusion. A recent review of all of these coefficients was made by Horseman et al. [7].

This paper is organized as follows. Section 2 is devoted to the theoretical determination of the coupling coefficients. The local transport equations corresponding to the electrical potential, the ionic concentrations, and the velocities are solutions of the Poisson–Boltzmann, the convection diffusion and the Stokes equations; these equations are numerically solved and integrated to obtain the macroscopic fluxes. Numerical results for various porous media correspond to the analytical solutions valid for circular Poiseuille flows when the capillary radius is replaced by a suitable length scale.

The material, the experimental procedure and the data are described in Section 3. Two samples of argilite extracted from a Callovo-Oxfordian formation were characterized. Permeability, conductivity, electro-osmotic coefficient, effective diffusion coefficient, osmotic coefficient, coefficient related to "membrane potential" and Soret coefficient measurements are described. Results are considered as functions of solute concentration, porosity and temperature in non-isothermal conditions. Data relative to the electrokinetic coefficients are compared to numerical and analytical results derived by [2] and [12].

2. General

The coefficients γ_{ij} defined by Eq. (1) can be derived by analysing the phenomena on the pore level. Such an analysis was performed for instance by [12] when there is no temperature gradient imposed on the medium. Let us summarize it briefly. Under such circumstances, transport is governed by three types of coupled equations. First, the concentration $n_i(\mathbf{R}, \mathbf{t})$ of each ith ion species is given by a convection–diffusion equation

$$\frac{\partial n_i}{\partial t} + \nabla\cdot\left(-D_i\nabla n_i - ez_i\frac{D_i}{kT}n_i\nabla\psi + n_i\mathbf{u}\right) = 0 \quad i = 1, 2, \ldots, N \tag{2}$$

where k is the Boltzmann constant ($= 1.38\times10^{-23}$ $\mathrm{m^2\,kg\,s^{-2}\,K^{-1}}$), t the time, D_i the diffusion coefficient of ion i, e the absolute value of the electron charge, z_i the valency, ψ the electric field, and $\mathbf{u}$ the fluid velocity.

Then, $\mathbf{u}$ and the pressure $p(\mathbf{R}, t)$ are governed by modified Stokes equations, since the Reynolds number is in most cases much less than unity:

$$\nabla\cdot\mathbf{u} = 0, \quad \mu\nabla^2\mathbf{u} = \nabla p + \rho\nabla\psi \tag{3}$$

where μ is the fluid viscosity and ρ the charge density.

Finally, $\psi(\mathbf{R}, \mathbf{t})$ is solution of the Poisson equation

$$\nabla^2\psi = -\frac{\rho}{\varepsilon_\mathrm{el}} = -\frac{e}{\varepsilon_\mathrm{el}}\sum_{i=1}^{N} n_i z_i \tag{4}$$

where ε_el is the fluid permittivity.

To be solved, the set of Eqs. (2) to (4) is subject to the following boundary conditions on the solid/fluid interface S:

$$\nu\cdot\mathbf{j}_i = 0, \quad \mathbf{u} = 0 \quad \text{and} \quad \psi = \zeta \tag{5}$$

where ν is the outward normal to the solid surface, and ζ the zeta potential.

These equations were linearized around equilibrium, made dimensionless, and solved by [9] (and the references therein) for homogeneous porous media that could be represented as spatially periodic media. The coefficients γ_{ij} ($i, j = 1, \ldots, 3$) can be derived by integrating the local fields over the unit cell.

The only cases which can be solved analytically, are the ones of a plane channel or of a circular tube of radius R_c. Let us recall the coefficients obtained in the latter case by Coelho et al. [8] and Marino et al. [9] (and references therein):

$$\gamma'_{11} = \frac{\gamma_{11}\mu e^2}{(\varepsilon_{el}kT\kappa)^2} = \frac{1}{2}(D'_1 + D'_2) - \frac{\zeta'}{\kappa\lambda' I_0(\kappa R_c)}\big((D'_1 - D'_2)I_1(\kappa R_c)\big) + 2\zeta'\left[\frac{\lambda'_3}{\kappa R_c I_0(\kappa R_c)} - I_1(\kappa R_c)\right] \quad (6a)$$

$$\gamma'_{12} = \gamma'_{21} = \frac{\gamma_{21}\mu}{\varepsilon_{el}\zeta K\kappa^2} = \zeta'\left[\frac{2I_1(\kappa\lambda')}{\kappa\lambda' I_0(\kappa\lambda')} - 1\right] \quad (6b)$$

$$\gamma'_{13} = \frac{\gamma_{13}\mu e}{\varepsilon_{el}(kT)^2} = \frac{1}{2}(D'_1 - D'_2) - \zeta'(D'_1 + D'_2)\frac{I_1(\kappa\lambda')}{\kappa\lambda' I_0(\kappa\lambda')} \quad (6c)$$

$$\gamma'_{23} = \frac{\gamma_{23}\mu\kappa^2}{kT} = 0 \quad (6d)$$

$$\gamma'_{33} = \frac{\gamma_{33}\mu e^2}{\varepsilon_{el}(kT)^2} = \frac{1}{2}(D'_1 + D'_2) - \zeta'(D'_1 - D'_2)\frac{I_1(\kappa\lambda')}{\kappa\lambda' I_0(\kappa\lambda')} \quad (6e)$$

where κ^{-1} is the Debye–Hückel length.

It is important to note that most numerical results obtained for various types of porous media were shown to be very close to the analytical results (6) when the radius of the tube is replaced by the characteristic length Λ' defined by

$$\Lambda' = \left(\frac{12.5K\sigma^\infty}{\sigma}\right)^{1/2} \quad (7)$$

where σ^∞ is the fluid conductivity (measured before any contact with argilite) and σ the macroscopic conductivity of the medium filled by the electrolyte. The definition of this length scale was inspired by the length scale Λ introduced by [9].

3. Experimental

The phenomenological coefficients γ_{ij} were measured in a series of one-dimensional experiments performed on porous specimens of thickness l and cross sectional diameter S separating two compartments each of volume V filled by aqueous solutions at different temperatures, pressures and electrical potentials with different concentrations of the same electrolyte. The concentration n expressed in m^{-3} is related to the molar concentration C expressed in mol m^{-3} by

$$C = n/N_a \quad (8)$$

where N_a is the Avogadro number ($= 6.02 \times 10^{23}$ mol^{-1}).

The relationships between the coefficients γ_{ij} and the measurable clay parameters can be summarized by:

$$\begin{pmatrix} \gamma_{11} & \gamma_{12} & \gamma_{13} & \gamma_{14} \\ \gamma_{21} & \gamma_{22} & \gamma_{23} & \gamma_{24} \\ \gamma_{31} & \gamma_{32} & \gamma_{33} & \gamma_{34} \\ \gamma_{41} & \gamma_{42} & \gamma_{43} & \gamma_{44} \end{pmatrix} = \begin{pmatrix} \sigma & \gamma_{12} & \gamma_{13} & \gamma_{14} \\ \gamma_{12} & \frac{K}{\mu} & \omega\frac{K}{\mu} & k_T \\ \frac{n}{kT}\gamma_{13} & \frac{n}{kT}\gamma_{23} & \bar{D} & n\bar{D}S_T \\ T\gamma_{14} & Tk_T & \frac{kT^2}{n^2}\gamma_{33}S_T & \lambda \end{pmatrix} \quad (9)$$

where σ is the electrical conductivity, K the permeability, μ the viscosity, ω the coefficient of osmotic efficiency, k_T the thermo-osmotic coefficient, $\bar{D}$ the macroscopic diffusion coefficient, S_T the Soret coefficient and λ the thermal conductivity.

3.1. Materials

The material, supplied to us by ANDRA, is a natural compact argilite extracted in eastern France from a Callovo-Oxfordian formation. The wellbore referred to as EST104 was sampled at two different levels. One at 483.6 m (EST104/2364) and the other at 505.15 m (EST104/2487). Both blocks were used to obtain solid cylinders of thickness 3 mm and diameter 12 mm, or powder. A SEM analysis of the argilite powder shows an heterogeneous structure with many aggregates; because of the careful crushing process to obtain powder from the original block, the average grain radius ranges from 1 to 10 μm. The variability of the samples is discussed in this issue by [14].

The solute was sodium chloride supplied by SIGMA (purity 99.5%). The solvent was pure water filtered by an HPCL Maxima unit. The concentration C was ranging between 10^{-4} and 10^{-2} mol l^{-1}.

The samples were equilibrated with the solutions for about a month and any additional and undesirable ion that appears during this initial equilibration phase can be eliminated. During the experiments, HPCL chromatography was performed and the concentration of any extra ions such as calcium was found negligible when compared to sodium.

The zeta potential ζ was estimated by measuring the electrophoretic mobility of clay particles in electrolyte solutions. Since the ratio between κ^{-1} and the particle dimension is small, the Smoluchowski formula [8] can

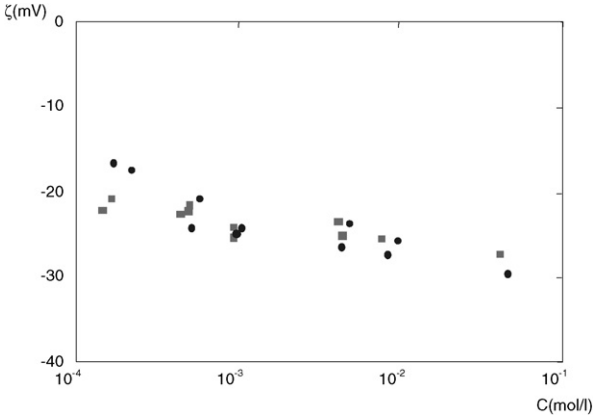

Fig. 1. The zeta potential ζ as a function of NaCl concentration C. Data are for: EST104/2364 (■) and EST104/2487 (●). The precision is about 15%.

Fig. 1. Potentiel ζ en fonction de la concentration C en NaCl. Les données sont pour : EST104/2364 (■) et EST104/2487 (●). La précision est d'environ 15%.

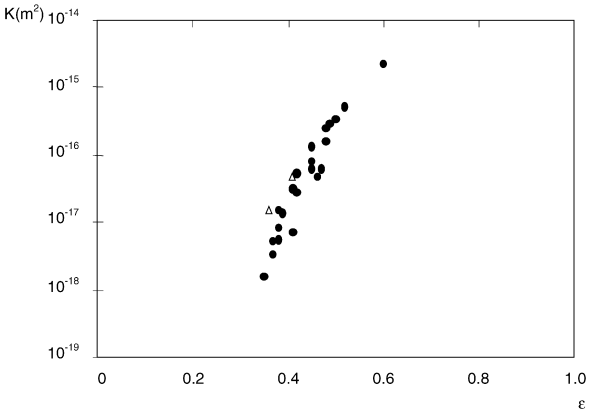

Fig. 2. The permeability K as a function of porosity ε. Data are for: argilite powder (●) and argilite original sample (△). The precision is about 34% and 24% for small and large porosities, respectively.

Fig. 2. Perméabilité K en fonction de la porosité ε. Les données sont pour : la poudre d'argilite (●) et l'échantillon initial (△). La précision est d'environ 34% et 24% pour les petites et grandes porosités.

be used for all particle shapes with an estimated precision of 10%:

$$\zeta = \frac{\mu u_e}{\varepsilon_{el}} \tag{10}$$

where u_e is the electrophoretic mobility.

Results for ζ in various NaCl solutions are displayed in Fig. 1. $|\zeta|$ is an increasing function of the concentration; it changes by only 7 mV (−18 to −25 mV) over a concentration range of 10^{-4} to 10^{-2} moll^{-1} at a constant pH value equal to 5.

3.2. Experimental determination of the coefficients K, σ and γ_{21} $(= \gamma_{12})$ in isothermal conditions

3.2.1. Experimental procedure

The experimental cell is detailed in [11] and [13]. The experiments were carried out at atmospheric pressure. The sample, whether it is the original compact rock or the powders, can be compacted or not by means of two porous disks. This compaction limits the swelling that is likely to occur with the addition of sodium chloride. Therefore, various porosities can be obtained for the same sample.

The permeability K was measured by generating a steady flow by means of a constant pressure difference $\Delta P \approx 2.4 \times 10^4$ Pa (0.24 bar). The mass of the outgoing water was measured during a given time in order to calculate the flow rate. Then, K was determined by using Darcy's law. Measurements were found reproducible.

The sample conductivity σ was measured by a classical method by imposing a constant dc voltage $\Delta V \sim$ 1 V between two bronze plates at a vanishingly small pressure difference ($\Delta P = 0$). Then, Ohm's law was used.

The electric current was observed to decrease during the measurement time when the electric potential difference is set, probably due to the formation of polarization layers on the electrodes. Simultaneously, a water flow rate Q_e was induced by ΔV and γ_{21} was obtained by:

$$\gamma_{21} = \frac{Q_e}{S}\frac{l}{\Delta V} \tag{11}$$

Q_e was determined from the slope of the straightline obtained from the linear fit of the collected liquid mass as a function of time during the first three minutes before it starts decreasing due to polarization.

3.2.2. Results and discussion

Results for permeability are displayed in Fig. 2. Note that the permeability obtained for the argilite original sample is in good agreement with the powder permeability.

In order to study the effects of the compaction pressure and κ, σ was measured for several porosities ε at fixed C, and for several C at fixed ε. It is more convenient to represent the experimental results in terms of the electric formation factor F, which is defined as:

$$F = \frac{\sigma_{fp}}{\sigma} \tag{12}$$

where σ_{fp} is the fluid conductivity after permeation. σ_{fp} was found equal to σ^∞ for C larger than 10^{-3} moll^{-1};

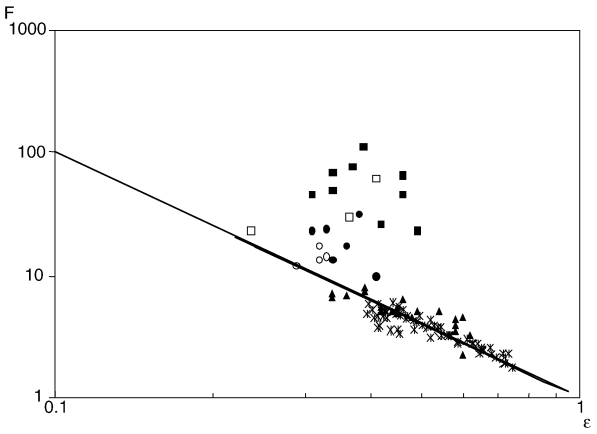

Fig. 3. The electric formation factor F (▲) and the diffusive formation factor $\bar{F}$ (■, □, ●, ○) as a function of the porosity ε. Data are for: EST104/2487 (●, ○) and EST104/2364 (■, □). Empty symbols are for $\overline{C} \leqslant 10^{-3}$ mol l^{-1}. Full symbols are for $\overline{C} > 10^{-3}$ mol l^{-1}. These data are compared to numerical results (⁎) obtained for various types of random packings [15]. The solid line is an approximate fit by Archie's law ε^{-2}.

Fig. 3. Facteur de formation électrique F (▲) et facteur de formation diffusif $\bar{F}$ (■, □, ●, ○) en fonction de la porosité ε. Les données sont : EST104/2487 (●, ○) et EST104/2364 (■, □). Les symboles vides sont pour $\overline{C} \leqslant 10^{-3}$ mol l^{-1}. Les symboles pleins sont pour $\overline{C} > 10^{-3}$ mol l^{-1}. Ces données sont comparées aux résultats numériques (⁎) obtenus pour les différents empilements aléatoires [15]. Le trait plein est une approximation par la loi d'Archie ε^{-2}.

however, for smaller concentrations, the two values were different. Results are displayed in Fig. 3. F is a decreasing function of ε and is independent of C.

In Fig. 3, these data are seen to be in very good agreement with the solution of the Laplace equation for various random packings [1]. They can be gathered by an Archie's law, $F = \varepsilon^{-2}$ when $0.1 \leqslant \varepsilon \leqslant 0.75$. Therefore, σ is essentially dominated by geometrical effects.

γ_{21} was measured by the same procedure as σ. γ_{21} is independent on C in the studied range; the mean value was found to be equal to $(3.3 \pm 1.2) \times 10^{-9}\,\mathrm{m^2\,V^{-1}\,s^{-1}}$ for $\varepsilon = 0.6$. At a fixed $C = 10^{-4}$ mol l^{-1}, γ_{21} increases with ε.

In Fig. 4, all results are gathered in the dimensionless form γ'_{21} as functions of $\kappa\Lambda'$, and compared to the numerical data recalled in Section 2. It is remarkable to note that the experimental data cluster around a single curve with very little dispersion. Moreover, the comparison with numerical results is very successful; therefore, the experimental data are also well approximated by Eq. (6b), which is a conclusion of high practical interest (cf. [15] for a detailed discussion).

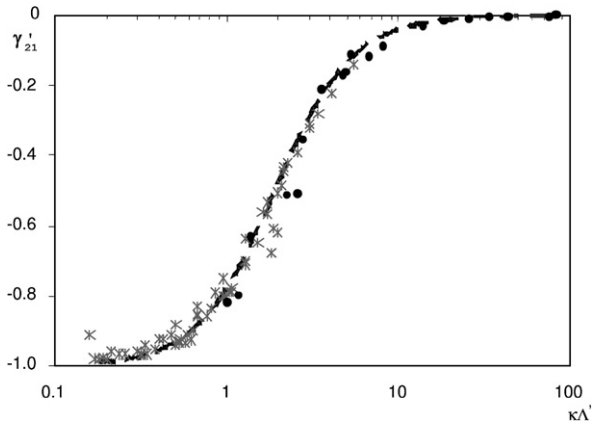

Fig. 4. The reduced coupling coefficient γ'_{21} as a function of $\kappa\Lambda'$. Data are for: argillite powder (●), numerical results obtained for various types of random packings (⁎). The dotted line is the least-square fit of Eqs. (7) and (6d).

Fig. 4. Coefficient de couplage réduit γ'_{21} en fonction de $\kappa\Lambda'$. Les données concernent : la poudre d'argillite (●), les résultats numériques (⁎) obtenus pour les différents empilements aléatoires. Le trait discontinu représente l'approximation aux moindres carrés – Éqs. (7) et (6d).

3.3. *Experimental determination of the coefficients γ_{13}, γ_{23}, γ_{33} and γ_{34}*

3.3.1. *Experimental procedure*

The experimental cell was described extensively in Refs. [13,16,17].

Two types of experiments have been performed; the samples were either compacted under different pressures by exerting a compaction pressure during the experiment (EST104/2487) or they were precompacted under a pressure equal to 46 bar before the experiment started (EST104/2364). Thermal regulation with a precision of ±0.5 °C was imposed by inserting coils of silicone tubings connected to two thermostats. The imposed temperature in each reservoir was measured by heat resistances. The temperature difference ΔT is ranging between 5 and 30 K.

The cell was initially assembled with either the less concentrated solution or the more concentrated one and the clay paste was brought to equilibrium with these concentrations. The minimal imbibition time is about 200 h. As a result, the sample was equilibrated with the solution and any additional and undesirable ion that appears during this initial equilibration phase can be eliminated.

Each experiment was divided into two periods. In the first one, a concentration gradient was imposed at a constant temperature of 25 °C. ΔC, ΔP and $\Delta\Psi_m$ were measured as functions of the time t. The second period starts after approximatively 200 h when a temperature

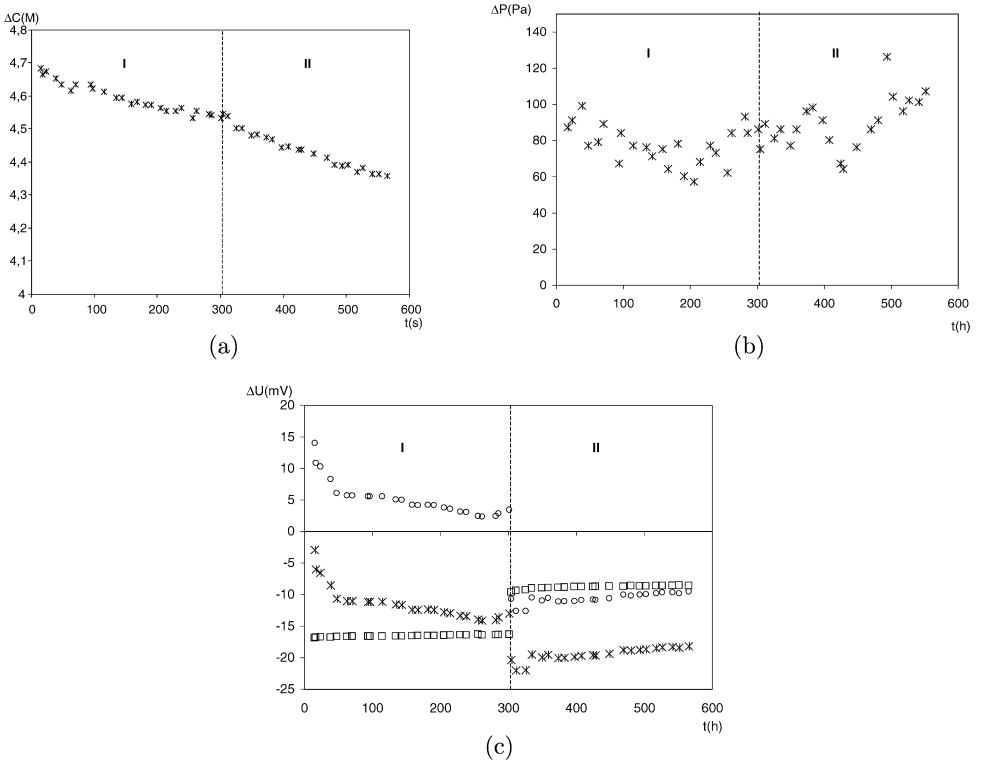

Fig. 5. A typical example of the evolution with time of the measured parameters: **(a)** $\Delta C = C_1 - C_2$. **(b)** ΔP. **(c)** $\Delta\Psi (= \Delta\Psi_{\text{meas}} - \Delta\Psi_{\text{N}})$ (○) obtained by subtracting from the measured potential difference $\Delta\Psi_{\text{meas}}$ (⁎), the electrode potential difference $\Delta\Psi_{\text{N}}$ (□). For period I, only ∇C is imposed and $T = 298$ K. For period II, ∇T is superimposed over ∇C.

Fig. 5. Exemple typique d'évolution temporelle des paramètres mesurés : **(a)** $\Delta C = C_1 - C_2$. **(b)** ΔP, **(c)** $\Delta\Psi$ $(= \Delta\Psi_{\text{mes}} - \Delta\Psi_{\text{N}})$ (○), obtenu en soustrayant la différence de potentiel d'électrode $\Delta\Psi_{\text{N}}$ (□) à la différence de potentiel mesurée. Pour la période I, seul ∇C est imposé et $T = 298$ K. Pour la période II, ∇T est superposé à ∇C.

difference was superposed over the concentration gradient, either in the same direction as the concentration gradient ($\nabla T \cdot \nabla C > 0$) or in the opposite direction ($\nabla T \cdot \nabla C < 0$). Again, ΔC, ΔP and $\Delta\Psi_{\text{m}}$ were measured as functions of t. T was also recorded in order to control its stability.

The total measured potential difference $\Delta\Psi_{\text{m}}$ induced by a concentration gradient consists of the electrode potential difference $\Delta\Psi_{\text{N}}$, and of the so-called membrane potential difference $\Delta\Psi$. Since $\Delta\Psi_{\text{N}}$ is given by the Nernst equation, in isothermal conditions, $\Delta\Psi$ can be expressed as:

$$\Delta\Psi = \Delta\Psi_{\text{m}} - \frac{RT}{F} \ln \frac{C_1}{C_2} \tag{13}$$

Fig. 5 shows typical evolutions of ΔC, $\Delta\Psi_{\text{m}}$ and ΔP with t. ΔC, $\Delta\Psi_{\text{m}}$ and ΔP vary linearly with t and decrease very slightly.

The weights m_{d} and m_{w} of the dry and wet sample are measured after the experiment in order to determine the porosity of the clay sample. The sample was dried in an oven at 100 °C during 24 h before the measurement of m_{d}.

3.3.2. *Determination of γ_{13}, γ_{23} and γ_{33} in isothermal conditions*

During period I, in the absence of any thermal gradient, ΔC, ΔP and $\Delta\Psi$ decrease with the same rate. Therefore, the ratios $\frac{\Delta\Psi}{\Delta C}$ and $\frac{\Delta P}{\Delta C}$ are constant, in agreement with the theory [6].

Since the seepage velocity is zero ($U(t) = 0$) in the present setup, and since there is no externally applied electrical field ($I(t) = 0$), the values of γ_{13} and γ_{23} can be deduced from the experimental values $\frac{\Delta P}{\Delta C}$ and $\frac{\Delta\Psi}{\Delta C}$ by using Eqs. (1a) and (1b)

$$\gamma_{13} = \gamma_{12} \frac{\Delta P}{\Delta C} + \gamma_{11} \frac{\Delta\Psi}{\Delta C} \tag{14a}$$

$$\gamma_{23} = -\gamma_{22} \frac{\Delta P}{\Delta C} - \gamma_{21} \frac{\Delta\Psi}{\Delta C} \tag{14b}$$

The global macroscopic diffusion coefficient $\bar{D}$ can be determined by considering the evolution of the con-

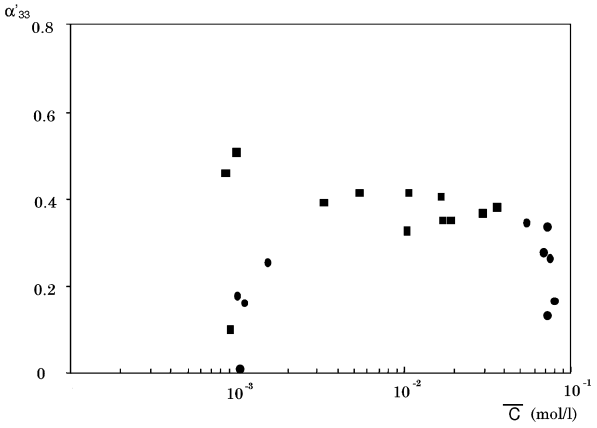

Fig. 6. The coupling coefficient α'_{33} as a function of the average concentration $\bar{C}$. Data are for: EST104/2487 (●) and EST104/2364 (■).

Fig. 6. Coefficient de couplage α'_{33} en fonction de la concentration moyenne. Les données sont : EST104/2364 (■) et EST104/2487 (●).

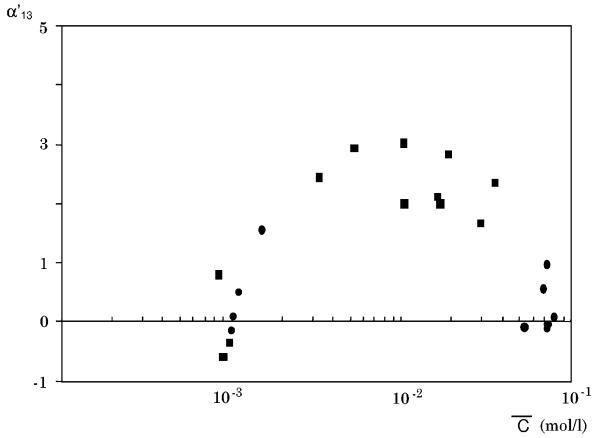

Fig. 7. The coupling coefficient α'_{13} as a function of the average concentration $\bar{C}$. Data are for: EST104/2487 (●) and EST104/2364 (■).

Fig. 7. Le coefficient de couplage α'_{13} en fonction de la concentration moyenne. Les données sont : EST104/2364 (■) et EST104/2487 (●).

centration profile (cf. [16]). $\bar{D}$ is related to γ_{33}. For non-isothermal conditions, the Soret coefficient was determined as described in [17].

3.3.3. *Analysis of γ_{13}, γ_{23} and γ_{33} in isothermal conditions*

$\bar{D}$ can be analysed by defining a diffusion formation factor:

$$\bar{F} = \frac{D_f}{\bar{D}} \tag{15}$$

where D_f is the diffusion coefficient in an infinite medium. These data are plotted in Fig. 3. If there were no influence of surface charges on the ions, one should obtain the same results for F and $\bar{F}$. This is not quite the case. $\bar{D}$ is relatively independent of concentration, but it depends on the sample; surface effects are indeed more important for EST104/2364.

The surface effects on $\bar{D}$ can be more precisely analysed by introducing the coefficient α'_{33}:

$$\alpha'_{33}\left(\frac{\gamma'_{33}}{D'_1+D'_2} - \frac{\gamma'_{33}(\zeta'=0)}{D'_1+D'_2}\right)\frac{1}{\zeta'} = -\frac{(D'_1-D'_2)}{(D'_1+D'_2)}\frac{I_1(\kappa R_c)}{\kappa R_c I_0(\kappa R_c)} \tag{16}$$

It was numerically shown to depend only on $\kappa\Lambda'$ by [12]. However, such a representation was not successful for the experimental data, which were found to be of the same order of magnitude, but with important differences, possibly due to experimental errors. The most satisfactory display for this quantity is given in Fig. 6 as a function of concentration.

The coefficient γ_{13}, related to the membrane potential, can be analyzed more precisely with the help of (6c) in order to eliminate the bulk effects; it may be written as:

$$\alpha'_{13}\left(\frac{\gamma'_{13}}{D'_1-D'_2} - \frac{\gamma'_{13}(\zeta'=0)}{D'_1-D'_2}\right)\frac{1}{\zeta'} = -\frac{(D'_1+D'_2)}{(D'_1-D'_2)}\frac{I_1(\kappa R_c)}{\kappa R_c I_0(\kappa R_c)} \tag{17}$$

Hence, division of γ'_{13} by $(D'_1 - D'_2)$ and F cancels the influence of the molecular diffusion coefficients and of the restricted geometry, respectively. However, the same remarks as for α'_{33} could be made and the representation in terms of $\kappa\Lambda'$ was not successful. In its stead, Fig. 7 displays α'_{13} as a function of concentration.

The coefficient γ_{31}, related to γ_{13} (see [12]), gives the magnitude of the total solute flux induced by the application of an electric field.

In Fig. 8, we have plotted γ'_{23} as a function of $\kappa\Lambda'$. It is obvious that γ'_{23} is very close to zero over the whole range of $\kappa\Lambda'$, indicating that osmosis is negligible.

The hyperfiltration (or inverse osmosis) coefficient γ_{32}, which is related to γ_{23} (see [12]), is a filtration process by which, upon application of an hydraulic gradient, solute concentration increases on the high-pressure side of the porous medium and a dilution of solute appears on the low-pressure side.

3.3.4. *Analysis of the Soret coefficient*

Fig. 9 displays the Soret coefficient S_T as a function of the applied temperature difference ΔT, the average concentration $\bar{C}$ and the average temperature $\bar{T}$. A linear temperature variation is likely to take place in the

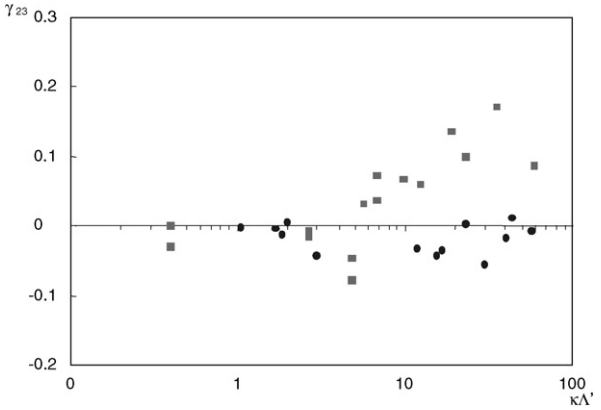

Fig. 8. The coupling coefficient γ'_{23} as a function of $\kappa\Lambda'$. Data are for: EST104/2487 (●) and EST104/2364 (■).

Fig. 8. Le coefficient de couplage γ'_{23} en fonction de $\kappa\Lambda'$. Les données sont : EST104/2364 (□) et EST104/2487 (●).

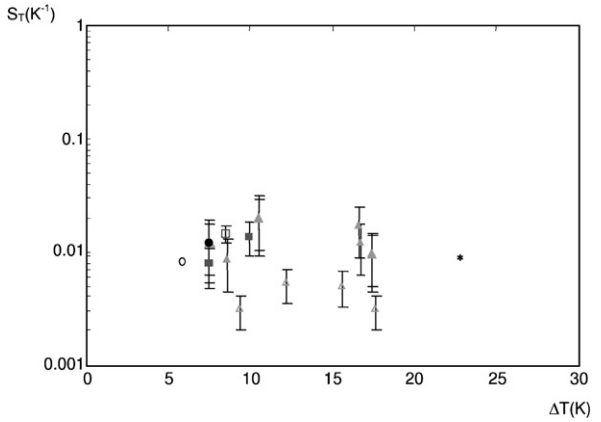

Fig. 9. The Soret coefficient S_T in compact clays as a function of temperature difference ΔT for various $\bar{C}$ and $\bar{T}$: $\bar{C} = 73$ mol m^{-3} and $\bar{T} = 25\,^{\circ}$C (△); $\bar{C} = 73$ mol m^{-3} and $\bar{T} = 33\,^{\circ}$C (◇); $\bar{C} = 1$ mol m^{-3} and $\bar{T} = 25\,^{\circ}$C (△); $\bar{C} = 1$ mol m^{-3} and $\bar{T} = 33\,^{\circ}$C (□); $\bar{C} = 54$ mol m^{-3} and $\bar{T} = 25\,^{\circ}$C (●); $\bar{C} = 30$ mol m^{-3} and $\bar{T} = 25\,^{\circ}$C (○) and $\bar{C} = 6$ mol m^{-3} and $\bar{T} = 25\,^{\circ}$C (∗).

Fig. 9. Coefficient de Soret S_T dans les argiles compactes en fonction de la différence de température ΔT pour diverses valeurs de $\bar{C}$ et $\bar{T}$. Les symboles sont définis ci-dessus.

sample, since in (1d), γ_{43} which corresponds to the Dufour effect, is very small. Moreover, thermal equilibrium is very rapidly obtained compared to diffusion.

It is important to note that we have omitted the absolute value in S_T and ΔT, due to the fact that $(S_T \Delta T)$ is always positive, indicating that the solute concentrates in the warmer region. Values obtained for $\bar{T}$ equal to 25 and 33 °C are approximatively the same. However, S_T depends slightly on $\bar{C}$. For $\bar{C} \approx 10^{-3}$ mol l^{-1}, S_T is close to 5×10^{-3} K^{-1}. For $\bar{C} > 10^{-3}$ mol l^{-1}, S_T is close to 1.3×10^{-2} K^{-1}.

Let us now compare our results with values obtained in a free medium for sodium chloride [3]. In the free medium, S_T is a slightly decreasing function of C. Indeed, for $C = 10^{-3}$ mol l^{-1}, S_T is equal to 2.3×10^{-3} K^{-1} and for $C = 5 \times 10^{-2}$ mol l^{-1}, equal to 1.6×10^{-3} K^{-1}. Therefore, our results are 5 to 10 times larger. In [18], the macroscopic Soret coefficient has been shown to be equal to the value in the free fluid for mica and glass powders. This difference is likely to be due to the finely divided nature of argilite with electrical effects coupled with temperature effects on the smallest pore scales.

4. Concluding remarks

The objective of this study was to analyze the behaviour of a compact clay, namely argillite, submitted to concentration, pressure, potential and temperature gradients and to compare the data to theoretical analysis, whenever possible. The coefficients were measured as functions of C and ε. Permeability ranges between 10^{-18} and 10^{-15} m^2 for ε between 0.35 and 0.6. The electrical formation factor is well represented by an Archie law ε^{-2}. Moreover, the macroscopic diffusion coefficient $\bar{D}$ ranges between 10^{-11} and 2×10^{-10} m^2 s^{-1}.

The osmotic coefficient γ_{23} is close to zero for all concentrations, indicating that osmosis has not a strong effect on solute and fluid transport.

γ_{21} ranges between 10^{-10} m^2 V^{-1} s^{-1} with a maximum value of 4×10^{-9} m^2 V^{-1} s^{-1}. The successful comparison with the analytical solution (6b) indicates that γ_{21} can be predicted in a simple way from K and F.

The coupling coefficient γ_{13} associated with membrane potential depends on the clay samples. Indeed, for EST104/2487, γ_{13} ranges between -5×10^{-31} and -10^{-29} A m^2. Negative values correspond to values in a free medium. For argillite EST104/2364, γ_{13} ranges between -9×10^{-30} and -2×10^{-29} A m^2 for $\kappa\Lambda' < 5$, and between 10^{-29} and 5×10^{-29} A m^2 for $\kappa\Lambda' > 5$. Positive values indicate that the clay efficiency is about 25–30%.

Non isothermal experiments show that solute transfer is enhanced by thermal diffusion. The Soret coefficients range between 5×10^{-3} and 1.3×10^{-2} K^{-1}. The positive sign indicates that solute concentrates in the warmer region.

References

[1] D. Coelho, J.-F. Thovert, P.M. Adler, Geometrical and transport properties of random packings of spheres and aspherical particles, Phys. Rev. E 55 (1997) 1959–1978.

[2] D. Coelho, M. Shapiro, J.-F. Thovert, P.M. Adler, Electro-osmotic phenomena in porous media, J. Colloid. Interface Sci. 181 (1996) 169–190.
[3] P. Costesèque, Sur la migration sélective des isotopes et des éléments par thermodiffusion dans les solutions. Applications de l'effet thermogravitationnel en milieu poreux, observations expérimentales et conséquences géochimiques, PhD thesis, University Paul-Sabatier, Toulouse, France, 1982.
[4] S.R. de Groot, P. Mazur, Non-Equilibrium Thermodynamics, North-Holland Publishing Company, Amsterdam, 1962.
[5] D.E. Elrick, D.E. Smiles, N. Baumgartner, P.H. Gronevelt, Coupling phenomena in saturated homo-ionic montmorillonite: I. Experimental, Soil Sci. Soc. Am. J. 40 (1976) 490–491.
[6] P.H. Gronevelt, D.E. Elrick, T.J.M. Blom, Coupling phenomena in saturated homo-ionic montmorillonite: III. Analysis, Soil Sci. Soc. Am. J. 42 (1978) 671–674.
[7] S.T. Horseman, J.J.W. Higgo, J. Alexander, J.F. Harrington, Water, gas and solute movement through argillaceous media, Report CC-96/1, Nuclear Energy Agency, 1996.
[8] R.J. Hunter, Zeta Potential in Colloid Science, Academic Press, New York, 1988.
[9] D.L. Johnson, J. Koplik, L. Schwartz, New pore-size parameter characterizing transport in porous media, Phys. Rev. Lett. 57 (1986) 2564–2567.
[10] A. Lerman, Geochemical Processes. Water and Sediment Environments, Wiley, New York, 1979.
[11] N. Mammar, M. Rosanne, B. Prunet-Foch, J.-F. Thovert, E. Tevissen, P.M. Adler, Transport properties of compact clays: I. Conductivity and permeability, J. Colloid Interface Sci. 240 (2001) 498–508.
[12] S. Marino, M. Shapiro, P.M. Adler, Coupled transports in heterogeneous media, J. Colloid Interface Sci. 243 (2001) 391–419.
[13] M. Paszkuta, Phénomènes de transport couplé dans les argiles du Callovo-Oxfordien, PhD thesis Institut de physique du Globe, Paris, 2005.
[14] P. Pellenard, J.-F. Deconninck, Mineralogical variability of Callovo-Oxfordian clays from the Paris Basin and the Subalpine Basin, C. R. Geoscience 338 (2006) 854–866.
[15] M. Rosanne, M. Paszkuta, J.-F. Thovert, P.M. Adler, Electro-osmotic coupling in compact clays, Geophys. Res. Lett. 31 (2004) 18614, doi:10.1029/2004GL020770.
[16] M. Rosanne, N. Mammar, N. Koudina, B. Prunet-Foch, J.-F. Thovert, E. Tevissen, P.M. Adler, Transport properties of compact clays. II. Diffusion, J. Colloid. Interface Sci. 260 (2003) 195–203.
[17] M. Rosanne, M. Paszkuta, E. Tevissen, P.M. Adler, Thermodiffusion in compact clays, J. Colloid. Interface Sci. 267 (2003) 194–203.
[18] M. Rosanne, M. Paszkuta, P.M. Adler, Thermodiffusional transport of electrolytes in compact clays, J. Colloid. Interface Sci. 299 (2006) 797–805.
[19] J.D. Sherwood, B. Craster, Transport of water and Ions through a clay membrane, J. Colloid. Interface Sci. 230 (2000) 349–358.
[20] E.C. Thornton, W.E. Seyfried Jr., Thermodiffusional transport in pelagic clay: Implications for nuclear waste disposal in geological media, Science 220 (1983) 1156–1158.